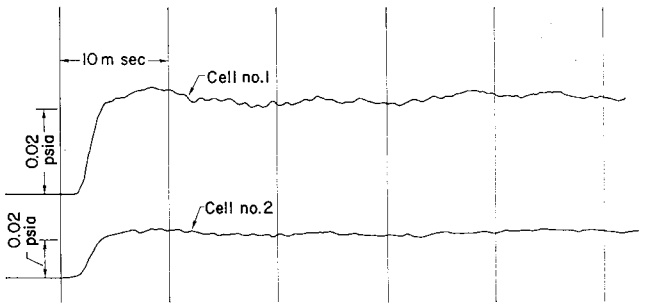

Fig. 3 Typical pressure traces.

tioned ahead of each pressure transducer (see Fig. 1) to act as a heat sink and thus keep the heating of the cell diaphragms to a minimum.

Pressures recorded over a period of 100 msec were on the order of 0.02 psia. A typical oscillograph pressure record is shown in Fig. 3. The time response of the system was limited to that of the galvanometer elements of the oscillograph, which was about 600 cps. The heat-sink screens ahead of the pressure transducers were apparently effective, as evidenced by the fact that the temperature rise of the cell diaphragm was less than 1°F. The resultant error in measurement due to diaphragm heating is not more than about 3% in this instance. The approximate levels of transmitted accelerations in the static-probe support system for this test are shown in Fig. 1. (Previous tests at much higher levels of shock-induced accelerations have shown that these transducers are relatively insensitive to "g" loads.) Pictures taken of the model during the test runs offer evidence that the flow through the probe interior was supersonic. The accuracy of the measured pressures is believed to be limited to the accuracy in reading the oscillograph traces, which is of the order of 5%.

Reference

[1] Dimeff, J., "A survey of new developments in pressure measuring techniques in the NACA," AGARD Conference, London (March 24–28, 1958).

Hypersonic Stability Derivatives of Blunted Slender Cones

Otto Walchner* and James T. Clay†
Aerospace Research Laboratories, Wright-Patterson Air Force Base, Ohio

Nomenclature

$d = 2R$	=	base diameter
$d_N = 2r_N$	=	nose diameter
dS	=	cone surface element (Fig. 1)
l	=	length, measured from the shoulder of the nose
M	=	pitching moment
n	=	pressure ratio $C_p/2\theta_c^2$
p_s	=	surface pressure
p_∞	=	ambient pressure
q	=	pitching velocity
r, x, ϕ	=	cylindrical coordinates (Fig. 1)
Re_l	=	Reynolds number based on l
V	=	velocity vector of c.g.
V_e	=	effective local velocity
V_N	=	velocity component perpendicular to the cone surface
α	=	static angle of attack
α_e	=	effective local angle of attack
θ_c	=	cone half angle
ρ	=	ambient density
ξ	=	nose bluntness ratio r_N/R
C_p	=	pressure coefficient $(p_s - p_\infty)/(\rho/2)V^2$
C_m	=	$M/(\rho/2)V^2R^2\pi l$ pitching moment coefficient
C_{m_α}	=	$\partial C_m/\partial\alpha$ static stability derivative
C_{m_q}	=	$\partial C_m/\partial(ql/V)$ damping derivative
C	=	$[\theta_c(1-\xi)/2\xi]^{1/2}$ correlation parameter

Received October 21, 1964

* Research Aerospace Engineer, Hypersonic Research Laboratory.

† Research Aerospace Engineer, Hypersonic Research Laboratory; also Captain, U. S. Air Force. Member AIAA.

Introduction

THE Newtonian impact theory with the pressure coefficient $C_p = 2(V_N/V)^2$ fails to predict the pressure distribution over slender, blunted cones and, therefore, must fail to predict the stability derivatives C_{m_α} and C_{m_q}. Thus, the occasionally observed agreement of one or the other derivative with the Newtonian prediction is believed to be accidental.

In the following, a semiempirical theory is presented based on Cheng's[1] analysis of slender blunted cones at zero angle of attack, while the tangent cone approximation is used to account for angle-of-attack effects. Quasi steady-state conditions are assumed to be valid.

Analysis

From Fig. 1 it can be seen that a cone element at the station x produces the differential pitching moment coefficient about the c.g.:

$$dC_m = \frac{2}{R^2\pi l}\int_{\phi=-\pi/2}^{\phi=+\pi/2}[r\sin\phi\,\sin\theta_c + (x - x_{c.g.})\cos\theta_c\sin\phi]C_p\,dS$$

where $dS = rd\phi dx/\cos\theta_c$. Substituting geometric relations from Fig. 1 and expressing the nose bluntness ratio by $\xi = r_N/R$, we obtain

$$dC_m = \frac{2}{\pi\tan\theta_c}\left[\frac{x}{l}(1-\xi\cos\theta_c)^2 + \xi\cos\theta_c(1-\xi\cos\theta_c)\right]\times\left[\frac{x}{l}(1+\tan^2\theta_c) - \frac{x_{c.g.}}{l} + \frac{\xi\cos\theta_c}{1-\xi\cos\theta_c}\tan^2\theta_c\right]\times d\left(\frac{x}{l}\right)\int_{-\pi/2}^{+\pi/2}C_p\sin\phi d\phi \quad (1)$$

Now, for slender cones with moderate nose bluntness

$$\cos\theta_c \sim 1 \qquad \tan\theta_c \sim \theta_c \qquad \frac{\xi}{1-\xi}\tan^2\theta_c \ll 1$$

$$\tan^2\theta_c \ll 1$$

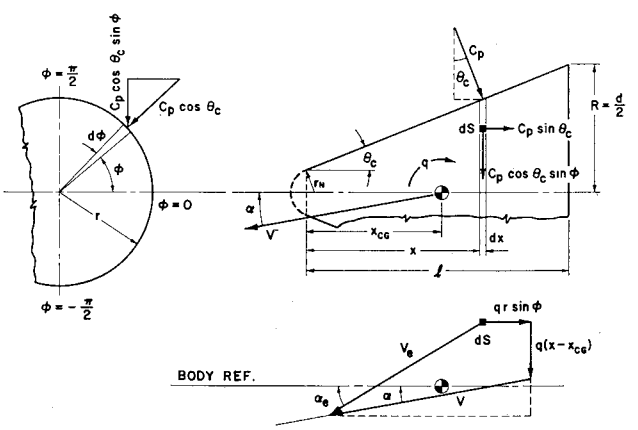

Fig. 1 Geometry of the investigated shape, pressure and velocity components for the surface element dS.

With these approximations, Eq. (1) reduces to

$$dC_m = \frac{2}{\pi\theta_c}\left[\frac{x}{l}(1-\xi)^2 + \xi(1-\xi)\right] \times \left[\frac{x}{l} - \frac{x_{c.g.}}{l}\right] d\left(\frac{x}{l}\right) \int_{-\pi/2}^{+\pi/2} C_p \sin\phi \, d\phi \quad (2)$$

Equation (2) may be evaluated if $C_p = C_p(\phi, \alpha, q, x/l \ldots)$ is known. Cheng theoretically obtained a correlation parameter for the surface pressures of blunted cones at zero angle of attack[1] which experiments as well as exact characteristic solutions[2, 3] have shown to exist. Thus, for zero angle of attack, C_p is known. For $\gamma = 1.4$ and for spherical noses, Fig. 2 shows the ratio $n = C_p/2\theta_c^2$ vs Cheng's parameter, $\theta_c(x/d_N)^{1/2}$.

Stability problems, however, require the knowledge of C_p as a function of ϕ at angles of attack. Using the tangent cone approximation, we can write

$$C_p = 2(\theta_c + \alpha_e)^2\left(n + \frac{\partial n}{\partial\theta_c}\alpha_e\right) \quad \text{for} \quad \phi = -\frac{\pi}{2} \quad (3a)$$

$$C_p = 2(\theta_c - \alpha_e)^2\left(n - \frac{\partial n}{\partial\theta_c}\alpha_e\right) \quad \text{for} \quad \phi \quad +\frac{\pi}{2} \quad (3b)$$

where α_e is the local effective angle of attack. For $-\pi/2 \leqq \phi \leqq \pi/2$, we assume that C_p has a sinusoidal variation of the form $C_p(\phi) = a - b\sin\phi$, where

$$a = 2\theta_c^2 n + 2\alpha_e^2 n + 4\theta_c\alpha_e^2(\partial n/\partial\theta_c)$$

$$b = 4\theta_c\alpha_e n + 2\theta_c^2\alpha_e\frac{\partial n}{\partial\theta_c}\left[1 + \left(\frac{\alpha_e}{\theta_c}\right)^2\right]$$

or for $(\alpha_e/\theta_c)^2 \ll 1$

$$b = 4\theta_c\alpha_e\left[n + \frac{1}{2}\theta_c\frac{\partial n}{\partial\theta_c}\right]$$

The pressure integral in (2) now becomes

$$\int_{-\pi/2}^{+\pi/2} C_p(\phi)\sin\phi \, d\phi = -2\pi\theta_c\alpha_e\left[n + \frac{1}{2}\theta_c\frac{\partial n}{\partial\theta_c}\right] \quad (4)$$

The local effective angle of attack α_e is composed of two parts, the static angle-of-attack α and the angle induced by the pitching velocity q. By inspection of the velocity diagram of Fig. 1 we find

$$\tan\alpha_e = \frac{V\sin\alpha + q(x - x_{c.g.})}{V\cos\alpha - qr\sin\phi}$$

and the effective velocity

$$V_e = \frac{q(x - x_{c.g.}) + V\sin\alpha}{\sin\alpha_e}$$

For small α and $ql/V \ll 1$, the foregoing expressions reduce to

$$\alpha_e = \alpha + \frac{ql}{V}\left(\frac{x}{l} - \frac{x_{c.g.}}{l}\right) \quad (5)$$

and $V_e = V$, respectively. Substituting (4) and (5) into (2), integrating over the length of the cone and taking the partial derivatives with respect to α and ql/V gives the contribution of the conical surface to the stability derivatives C_{m_α} and C_{m_q}. It remains to add the contribution by the spherical nose. The Newtonian impact theory is applicable for the rounded nose, and the derivatives are readily available from Ref. 4. Using the Nomenclature of the present report, the nose contributions to C_{m_α} and C_{m_q} of Ref. 4 become $+\xi^2(x_{c.g.}/l)$ and $-\xi^2(x_{c.g.}/l)^2$, respectively. The analysis now yields the derivatives

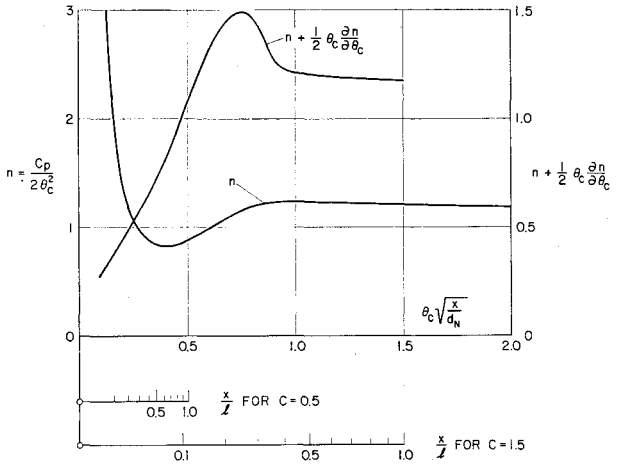

Fig. 2 Cone surface pressure correlation ($\gamma = 1.4$, spherical noses), defined by $n = C_p/2\theta_c^2$ vs Cheng's parameter $\theta_c(x/d_N)^{1/2}$ at zero angle of attack (Refs. 2, 3). Included are the term $[n + \frac{1}{2}\theta_c(\partial n/\partial\theta_c)]$ from Eqs. (6) and (7) and the axial scales x/l for two cone families defined by $C = 0.5$ and 1.5.

$$C_{m_\alpha} = +\xi^2\frac{x_{c.g.}}{l} - 4\int_0^1\left[\frac{x}{l}(1-\xi)^2 + \xi(1-\xi)\right] \times \left[\frac{x}{l} - \frac{x_{c.g.}}{l}\right]\left[n + \frac{1}{2}\theta_c\frac{\partial n}{\partial\theta_c}\right] d\left(\frac{x}{l}\right) \quad (6)$$

$$C_{m_q} = -\xi^2\left(\frac{x_{c.g.}}{l}\right)^2 - 4\int_0^1\left[\frac{x}{l}(1-\xi)^2 + \xi(1-\xi)\right] \times \left[\frac{x}{l} - \frac{x_{c.g.}}{l}\right]^2\left[n + \frac{1}{2}\theta_c\frac{\partial n}{\partial\theta_c}\right] d\left(\frac{x}{l}\right) \quad (7)$$

To evaluate Eqs. (6) and (7), the term $[n + \frac{1}{2}\theta_c(\partial n/\partial\theta_c)]$ must be known as a function of x/l. In Fig. 2 we have added the curve $[n + \frac{1}{2}\theta_c(\partial n/\partial\theta_c)]$, where

$$\theta_c\frac{\partial n}{\partial\theta_c} = \theta_c\frac{dn}{d[\theta_c(x/d_N)^{1/2}]}\left(\frac{x}{d_N}\right)^{1/2}$$

Writing Cheng's parameter in terms of ξ and x/l,

$$\theta_c(x/d_N)^{1/2} = [\theta_c(1-\xi)/2\xi]^{1/2}(x/l)^{1/2}$$

it is clear that there are families of blunted cones defined by the parameter

$$[\theta_c(1-\xi)/2\xi]^{1/2} = C$$

and that the x/l distribution of $[n + \frac{1}{2}\theta_c(\partial n/\partial\theta_c)]$ is the same for all members of a family defined by one value of the parameter C. For illustration, the scale x/l is included in Fig. 2 for two families defined by $C = 0.5$ and 1.5.

For large values of C the cone pressure distribution approaches that predicted by Newtonian theory. Applying Newtonian theory to this analysis, i.e., $n = 1$ and $\partial n/\partial\theta_c = 0$, Eqs. (6) and (7) integrate immediately to give

$$C_{m_{\alpha_{Newt}}} = -\tfrac{4}{3} + \tfrac{2}{3}\xi(1+\xi) + x_{c.g.}/l\,(2 - \xi^2) \quad (8)$$

$$C_{m_{q_{Newt}}} = -1 + \tfrac{1}{3}\xi(2+\xi) + \tfrac{4}{3}(x_{c.g.}/l) \times [2 - \xi(1+\xi)] - (x_{c.g.}/l)^2(2 - \xi^2) \quad (9)$$

Equations (8) and (9) are in agreement with the Newtonian derivatives based on $C_p = 2(V_N/V)^2$ from Refs. 4 and 5, if $\cos^2\theta_c = 1$.

Results

Equations (6) and (7) have been evaluated for $x_{c.g.}/l = 0.5$ using the curve for $n + \frac{1}{2}\theta_c(\partial n/\partial\theta_c)$ shown in Fig. 2 and for three bluntness ratios, $\xi = 0.1$, 0.2, and 0.3. The calculated derivatives are plotted in Fig. 3 vs C, and the Newtonian values from Eqs. (8) and (9) are included. The damping derivatives C_{m_q} as defined in this note‡ depend mainly on C and are practically independent of ξ for the chosen c.g. position. For other c.g. locations the variations of C_{m_q} with ξ is

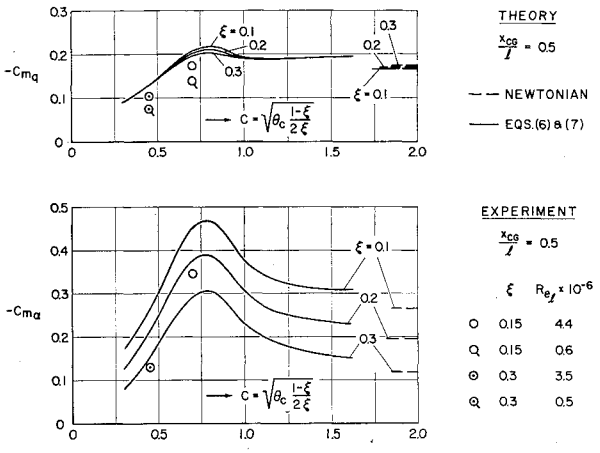

Fig. 3 Stability derivatives vs C, evaluated from Eqs. (6–9) for $x_{c.g.}/l = 0.5$. Comparison with some experiments.[6]

greater. The static derivatives C_{m_α} depend on C and also on ξ. Some recent experimental results from small amplitude forced oscillation tests at zero trim angle of attack, Mach 10, $\theta_c = 10°$, $\xi = 0.15$, and 0.3[6] are also shown in Fig. 3. The trend of decreasing derivatives found experimentally for cones with values of $C < 0.7$ is predicted by the theory. Quantitatively the experimental derivatives are lower than the theoretical values. Note that the obvious agreement of one or the other measured derivative with the Newtonian prediction is purely accidental. The evident Reynolds number effect on the damping derivatives indicates that there is an additional viscous effect that is not included in the present theory. Tests are presently being conducted at the Aerospace Research Laboratory to verify experimentally the assumptions and results of this theory.

References

[1] Cheng, H. K., "Hypersonic flow with combined leading edge bluntness and boundary-layer displacement effect," Cornell Aeronautical Lab. Rept. AF-1285-A-4 (August 1960).

[2] Griffith, B. J. and Lewis, C. H., "A study of laminar heat transfer to spherically blunted cones and hemisphere-cylinders at hypersonic conditions," Arnold Engineering Development Center Tech. Doc. Rept. AEDC TDR 63-102 (June 1963).

[3] Wagner, R. D. and Watson, R., "Induced pressures and shock shapes on blunted cones in hypersonic flow," NASA TND-2182 (March 1964).

[4] Fisher, L. R., "Equations and charts for determining the hypersonic stability derivatives of combinations of cone frustums computed by Newtonian impact theory," NASA TND-149 (November 1959).

[5] Tobak, M. and Wehrend, W. R., "Stability derivatives of cones at supersonic speeds," NACA TN 3788 (September 1956).

[6] Hodapp, A. E., Jr., Uselton, B. L., and Burt, G. E., "Dynamic stability characteristics of a 10-degree cone at Mach number 10," Arnold Engineering Development Center, AEDC TDR 64-98 (May 1964).

‡ Some authors use the cone base diameter as the reference length for defining C_{m_q} and C_{m_α}, and some use the actual cone length. The correlation shown herein does not exist when C_{m_q} and C_{m_α} are defined by using the base diameter.

Thermodynamics of Turbine and Piston Rankine Space Power Cycles

P. C. Chang* and J. R. Powell†
Brookhaven National Laboratory, Upton, N. Y.

Nomenclature

P = pressure, atm
T_B = boiler temperature, °F
T_C = condenser temperatures, °F
V_F = final specific volume, ft³/lb
V_0 = initial specific volume at boiler conditions, ft³/lb
η = thermal cycle efficiency

THE usual alkali metal space power cycle is the Rankine, with continuous flow turbines. However, noncontinuous flow machines, e.g., the conventional steam piston engine, are possible. Several types of noncontinuous flow MHD generators are being studied[1] in which either a liquid metal or MHD lubricated solid piston is driven in reciprocating motion through a magnetic field by metal vapor. These generators are mechanically and electrically attractive, but compactness requires high operating pressures and low expansion ratios, with some irreversible throttling to the condenser. A study was made comparing thermal efficiency and weight for turbines and pistons with varying expansion ratios. Potassium was chosen as a typical alkali metal working fluid. Its thermodynamic properties are the best known, but still quite incomplete. The T-S diagram was constructed with the following data and assumptions:

1) The saturated liquid T-S curve was drawn using C_s data from work at Battelle[2] with extrapolation above 2100°F.

2) Critical constants were taken from Grosse.[3]

3) Entropy of vaporization was assumed equal to experimental values for mercury at corresponding reduced temperatures, following Grosse.[3]

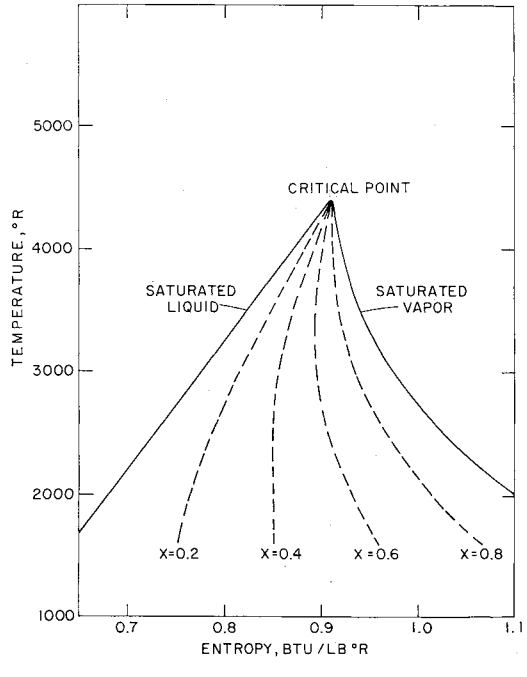

Fig. 1 T-S diagram for potassium.

Received October 26, 1964. This work was done under the auspices of the U. S. Atomic Energy Commission. The authors wish to thank Ann Potter for her aid in computation.

* Research Assistant.
† Nuclear Engineer.